RSC Advances

PAPER

View Article Online
View Journal | View Issue

Cite this: *RSC Adv.*, 2019, **9**, 23061

Room-temperature production of bio-based aldehydes from vegetable oil-derived epoxide *via* H_2WO_4@Al-MCM-41 as recyclable catalyst

Libo Peng, Qinglong Xie, Yong Nie, Xuejun Liu, Meizhen Lu * and Jianbing Ji

The oxidative cleavage of vegetable oils and their derivatives to produce bio-based aldehydes is a potentially useful process, although the aldehyde products are readily oxidized to carboxylic acids and thus seldom obtained in high yields. The present study developed a room-temperature method for the synthesis of bio-aldehydes *via* the oxidative cleavage of vegetable oil-derived epoxides, using H_2WO_4 as the catalyst, H_2O_2 as the oxidant, and *t*-BuOH as the solvent. Reactions were carried out at temperatures ranging from 25 to 35 °C for 3.5–10.5 h, and provided >99% conversion and >90% aldehyde yield. In particular, an approximately 97% yield was obtained at 25 °C after 10.5 h. As the reaction proceeded, the H_2WO_4 dissolved to form a W-containing anion. Several mesoporous Al-MCM-41 materials having different Si/Al ratios were hydrothermally synthesized and used as adsorbents to recover the catalyst by adsorbing these anions. The adsorption capacity of the Al-MCM-41 was found to increase with decreases in the Si/Al ratio. The Al-MCM-41 had little effect on the oxidative cleavage reaction at 25 °C, and thus could be directly added to the reaction system. The excellent anion adsorption performance of the Al-MCM-41 greatly improved the reusability of the H_2WO_4 catalyst. When using the Al-MCM-41 with the best adsorption performance, there was no significant decrease in the activity of the catalyst following five reuses.

Received 10th June 2019
Accepted 20th July 2019

DOI: 10.1039/c9ra04348a

rsc.li/rsc-advances

1. Introduction

Vegetable oils are an important biomass-derived energy source[1] that can also be used in the food and chemical industries. Historically, these oils have typically been employed as foods, but more recently have been used to produce bio-based chemicals. This transition is due to concerns regarding limited petroleum reserves and increased environmental awareness. The American Oil Chemists' Society has assessed the usages of nine major vegetable oils: coconut, cottonseed, olive, palm, palm kernel, peanut, rapeseed, soybean, and sunflower in recent years.[2] Interestingly, between 1999 and 2012, the portion of such oils employed for applications other than human food has increased from 10.5% to 23.9%.[3]

The vegetable oils not used for foods are typically processed into high value-added bio-based products that are both biodegradable and nontoxic, often based on epoxidation reactions.[4] Epoxidized vegetable oils have numerous commercial applications, including as additives in lubricants, costabilizers and plasticizers in polymers, stabilizers in chlorine-containing resins, pharmaceutical components and biofuel additives.[5,6] There are various approaches to the epoxidation of these oils. In classic practice, the industrial scale epoxidation of vegetable oil, such as unsaturated fatty acid methyl esters (UFAMEs), is carried out by reacting the C=C double bonds in the oil with a percarboxylic acid (generally peracetic acid or performic acid) generated *in situ* during the reaction.[7] Other methods involve highly active catalytic systems, including Ti/silica,[8] CoCuAl double layered hydroxides,[9] VO supported on Indion 130,[10] $Mo(O)_2Cl_2(H_2biim)$ (H_2biim = 2,2′-bisimidazole) supported on an ionic liquid ([BMIM][PF_6]),[11] methyltrioxorhenium,[12] tungsten-containing heteropolyacids,[13] lipases,[14] $H_5PV_2Mo_{10}O_{40}/Na_2SO_3$ (ref. 15) and so on.

Vegetable oils can also be oxidatively cleaved into the corresponding aldehydes, which have various applications. As an example, methyl oleate can be oxidized and cleaved to synthesize nonanal and methyl 9-oxononanoate. The nonanal can be used as a spice or to prepare 100% bio-based surfactants *via* the reductive alkylation of polyols,[16,17] while the methyl 9-oxononanoate can be converted to polymer monomers by hydrogenation or reductive amination.[18] Normally, the oxidative cleavage of UFAMEs is performed using ozonolysis and/or a metal catalyst, such as Cr,[19] Mo,[20] Ru,[21] Os[22] or W.[23] Although these methods provide excellent conversions, the products are primarily carboxylic acids rather than aldehydes, which tend to appear only as intermediates.[2] This occurs because the C=C bonds in UFAMEs are highly stable, such that the oxidative cleavage of these compounds requires harsh reaction conditions, including high temperatures, long

Institute of Chemical Engineering, Zhejiang University of Technology, Zhejiang Province Key Laboratory of Biofuel, Biodiesel Laboratory of China Petroleum and Chemical Industry Federation, No. 18 Chaowang Road, Hangzhou, Zhejiang 310014, China. E-mail: zjutluzhen@163.com; Fax: +86 571 88320043

durations and strong oxidants such as O_3, $NaIO_4$ and $KMnO_4$. Consequently, the as-formed aldehydes are easily further oxidized to carboxylic acids.[24]

To obtain high yield of aldehydes from UFAMEs, it is vital to avoid or at least lessen the over-oxidation of aldehydes, and various novel strategies have been proposed for this purpose. Louis *et al.*[18] developed an oxydoreductive cleavage using PPh_3 or H_2 + Pd/C that reduces the ozonides of UFAMEs to generate aldehydes and gives complete conversion together with >90% aldehydes yield. Deruer *et al.*[25] used a thiazolylidene catalyst to cleave the α-hydroxy ketone derived from methyl oleate into the corresponding aldehydes at 150 °C and reported a 60% conversion and 40% yield. Other catalyst/oxidant systems with high selectivity for aldehydes have also been designed, including $[Fe(OTf)_2$(mix-bpbp)](bpbp = *N*,*N*′-bis(2-picolyl)-2,2′-bipyrrolidine)/H_2O_2 + $NaIO_4$,[26] niobium(v) oxide/H_2O_2,[27] nano-RuHAP(HAP = hydroxyapatite)/$NaIO_4$ (ref. 28) and alkylated polyethyleneimine/$Na_3\{PO_4[WO(O_2)_2]_4\}$/$H_2O_2$.[29] In previous work by our own group,[30] epoxy fatty acid methyl esters (EFAMEs) were cleaved into the corresponding free aldehydes using WO_3 and H_2O_2. The feedstock conversion obtained from this process was >99% at a reaction temperature of 80 °C, but the selectivity for aldehydes was approximately 80% and thus unsatisfactory. Therefore, further research is required to improve the aldehyde selectivity associated with this technique.

To the best of our knowledge, the oxidative cleavage of epoxy group with W-based catalysts and H_2O_2 proceeds *via* the initial hydrolysis of epoxy groups to vic-diols, followed by oxidation to give aldehydes or carboxylic acids (Scheme 1(a)).[2,31,32] Acidic conditions enhance the oxidative cleavage of epoxides by promoting the hydrolysis of epoxy groups (Scheme 1(b)).[33,34] Thus, the use of H_2WO_4 instead of WO_3 as the catalyst could potentially provide better results. However, H_2WO_4 may also react with H_2O_2 to form soluble W-containing anions,[35] thus reducing the extent to which the catalyst can be recovered. For this reason, in prior work, dissolved W-containing anions were adsorbed using mesoporous tin dioxide to regenerate catalyst.[23] However, the pore structure in this dioxide is unstable, and this material also has a low specific surface area and is costly to prepare compared to more common mesoporous materials such as SiO_2. Typically, in the case that the point of zero charge (PZC) of a mineral is higher (lower) than the pH of a solution, the mineral will interact with hydrogen (hydroxide) ions in the solution to generate positive (negative) charges on its surface (Scheme 2), such that it is able to adsorb anions (cations). For this reason, a mineral having a high PZC (such as Al_2O_3, MgO or ZnO) can be used to adsorb W-containing anions from the reaction products resulting from a mixture of H_2WO_4, H_2O_2 and EFAMEs.[36,37]

Because H_2O_2 can be decomposed by most metal oxides,[38] it is beneficial to disperse the metal oxide well to the solid that can coexist with H_2O_2 (just like SiO_2) to reduce the amount of metal. Among the various metal-doped SiO_2 materials, Al-MCM-41 has been widely studied because its Al content is readily adjustable and it has a suitable mesoporous structure.[39] Due to their unique features, including high surface areas, large pores, narrow pore size distributions and high pore volumes, mesoporous materials such as Al-MCM-41 provide increased accessibility of the reacting species to active sites on internal surfaces. Thus, these materials are of interest with regard to applications involving relatively large molecules such as long chain alkanes and lipids.[40]

In the present investigation, methyl 9,10-epoxystearate (**1**) derived from methyl oleate was used as a model to study the oxidative cleavage of EFAMEs into bio-based aldehydes, using H_2WO_4 as the catalyst, H_2O_2 as the oxidant and *t*-BuOH as the solvent. To avoid side reactions and the thermal decomposition of H_2O_2, all reactions were performed at or close to room temperature. Subsequently, mesoporous Al-MCM-41 materials having different PZC values (due to varying Si/Al ratios) were prepared *via* direct mixed-gel synthesis and used as adsorbents to recover the catalyst.

2. Experimental

2.1. Raw materials

The methyl oleate used in this work was provided by Shandong Baiqian Chemical Co. The other reagents were purchased from Aladdin Co. and were of analytical grade. The epoxide **1** was prepared from methyl oleate through a previously reported method.[41] It was composed of epoxide **1** (about 80 wt%), methyl octadecanoate (about 14 wt%) and methyl palmitate (about 6 wt%).

2.2. Oxidative cleavage of methyl 9,10-epoxystearate

10 mmol of epoxide **1**, 0.17 mmol of H_2WO_4, 5 ml of *t*-BuOH and 100 mg of Al-MCM-41 were stirred at 25–35 °C until uniform followed by 12 mmol of H_2O_2 (30 wt%) was added dropwise. The resulting mixture was continued to stir for 3.5–10.5 h. The liquid products were then obtained by centrifugation to remove Al-MCM-41 that adsorbed tungsten, and the solid was recovered through washed with *t*-BuOH and dried at room-temperature.

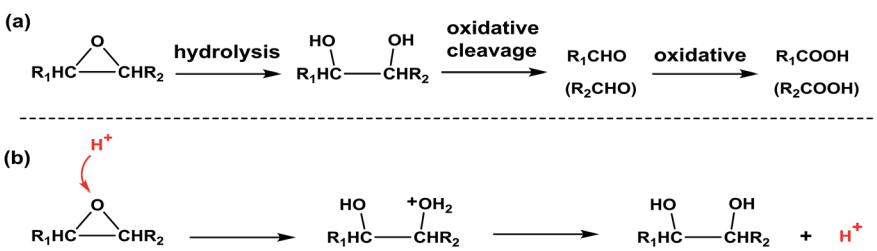

Scheme 1 The mechanism of oxidative cleavage of epoxy group by tungsten catalysts and H_2O_2.

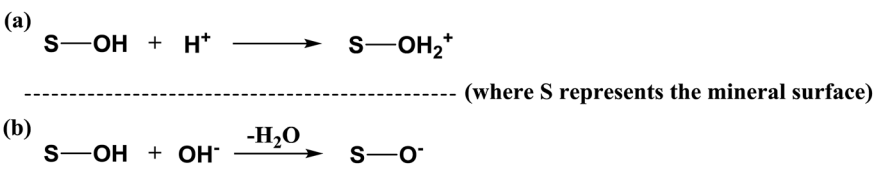

Scheme 2 Interaction between mineral and H^+ or OH^- in solution.

2.3. Product analysis

Qualitative analysis of the product was performed by a gas chromatography-mass spectrometry (GC-MS, Agilent 7890A/5975C) equipped with a DB-5 capillary column (30 m × 0.25 mm × 0.25 μm). Helium with a purity of 99.99% was used as the carrier gas. The oven temperature was held at 50 °C for 3 min, and then raised to 150 °C at a rate of 10 °C min^{-1} and held for 1 min, and then raised to 220 °C at a rate of 10 °C min^{-1} and held for 3 min, and finally raised to 280 °C at a rate of 10 °C min^{-1} and held for 10 min. All of the peaks were determined according to the National Institute of Standards and Technology (NIST) library.

The product was analyzed by a gas chromatograph (Shimadzu, GC-2014) equipped with a DB-5 capillary column (30 m × 0.25 mm × 0.25 μm) and a flame ionization detector (FID). The oven temperature was similar to the qualitative analysis of the product using GC-MS. The quantification of feedstock and product was conducted using the internal standard method with undecanal as the internal standard. The feedstock conversion and product yield were calculated using the following equations:

$$\text{Feedstock conversion} = (\text{feedstock reaction amount/feedstock feed amount}) \times 100\%;$$

$$\text{Product selectivity} = (\text{amount of feedstock converted to the target product/feedstock reaction amount}) \times 100\%;$$

$$\text{Product yield} = \text{feedstock conversion} \times \text{product selectivity}.$$

2.4. Preparation of Al-MCM-41

According to the previous work,[40] the Al-MCM-41 with different Si/Al molar ratios from 10 to 90 were synthesized from a gel molar composition of 1.00 Si : *x*Al : 0.25 CTAB : 0.20 TMAOH : 40H_2O, where $x = 0.1000$, 0.0333, 0.0200, 0.0143 and 0.0111, corresponding to Si/Al molar ratios of 10, 30, 50, 70 and 90, respectively. In more detail, cetyltrimethylammonium bromide (CTAB, >99 wt%) and tetramethylammonium hydroxide (TMAOH, >97 wt%) were dissolved in distilled water under stirring at 35 °C. Then, the aluminum isopropoxide (>98 wt%) and tetraethyl orthosilicate (TEOS, >98 wt%) were slowly added into the template solution under stirring for 1 h. After further stirring for 1 h, the obtained gel mixtures were aged for 72 h at room temperature. The solid products were then filtrated, washed with distilled water until the pH of the filtrate was 7, and dried at 70 °C for 12 h. Finally, Al-MCM-41 were obtained after calcining in air at 550 °C for 8 h. The as-synthesized Al-MCM-41 were noted as Al-MCM-41-*y*, where $y = 10$, 30, 50, 70 and 90. In addition, the corresponding Al-free sample, designated as MCM-41, was prepared as outlined in the above procedure without the addition of aluminum isopropoxide.

2.5. Characterization of Al-MCM-41

The actual Si/Al ratios of Al-MCM-41-*y* were measured using an inductively coupled plasma mass spectrometer (ICP-MS) after dissolving the samples in hydrofluoric acid.

Powder X-ray diffraction (XRD) patterns were obtained using a PANalytical X'Pert Pro powder diffractometer with Cu Kα (λ = 0.154056 nm, 40 kV, 40 mA) radiation.

The specific surface area, pore volume and average pore size were measured by N_2 adsorption at 77 K using an Micromeritics ASAP-2020-PLUS-HD88 instrument. Specific surface area was calculated using the standard Brunauer–Emmet–Teller (BET) model. The total pore volume was determined from the amount of N_2 adsorbed at a relative pressure p/p_0 of 0.99. Pore size distribution curve was calculated from the adsorption branch of the isotherm using the Barrett–Joyner–Halenda (BJH) method.

The morphology and the pore structure information were studied by transmission electron microscopy (TEM) using a Tecnai G2 F30 S-Twin microscope. The sample was dispersed in ethanol in an ultrasonic bath for several minutes before deposited onto a Cu grid followed by being dried under an infrared heat lamp.

The contents of Brønsted and Lewis acid sites of MCM-41 and Al-MCM-41 were determined by the *in situ* Fourier transform infrared spectroscopy of adsorbed pyridine (Py-FTIR) using a Thermo fisher Nicolet iS50 spectrometer. The sample was pressed into a self-supporting disk and placed in a stainless-steel IR cell equipped with CaF_2 windows. Initially, sample was pretreated in He flow at 300 °C for 2 h to remove any adsorbed impurities, then the cell temperature was lowered to 50 °C and a spectrum was recorded as background. Subsequently, pyridine was introduced and adsorbed on sample for 2 h at 50 °C. After pyridine adsorption, sample was evacuated for 1 h at 50 °C to remove all physically adsorbed pyridine. Four spectra were recorded under He flow at the following stages: (1) after 1 h evacuation at 50 °C, (2) after desorption at 150 °C for 1 h, (3) after desorption at 250 °C for 1 h, and (4) after desorption at 350 °C for 1 h. The concentrations of Brønsted and Lewis acid sites were calculated by integrating the absorption bands at 1545 cm^{-1} and 1455 cm^{-1}, respectively and using the molar extinction coefficients reported by Emeis.[42]

2.6. Determination of PZC values

The PZC values of MCM-41 and Al-MCM-41 were determined using a salt titration technique.[43] In each experiment, 2 g

samples were placed in each of seven 50 ml glass tubes. Subsequently, deionized water was added and the pH values of the resulting suspensions were adjusted to span the expected pH_0 value, using either 0.1 mol L^{-1} HC1 or 0.1 mol L^{-1} NaOH. In each case, the final volume was 20 ml. Each sample was subsequently allowed to equilibrate for four days with occasional stirring, after which the equilibrium pH was recorded and designated as pH_1. Following this, 0.5 ml of a 2 mol L^{-1} NaC1 solution was added and the tube was agitated using a reciprocal shaker for 3 h, after which the pH value was recorded as pH_2. For each tube, ΔpH ($=pH_2 - pH_1$) was calculated and the ΔpH values were plotted *versus* pH_1 to determine the point at which $\Delta pH = 0$. The corresponding pH equaled the PZC value for the sample.

2.7. Adsorption of W-containing anions by Al-MCM-41

Experiments were performed to assess the adsorption of W-containing anions by the Al-MCM-41. In these experiments, 1.7 mmol of H_2WO_4 and 120 mmol of H_2O_2 were combined and stirred until the H_2WO_4 was completely dissolved, after which 100 mg of Al-MCM-41 was introduced into the solution, followed by continuous stirring for 4 h at ambient temperature. Thereafter, the liquid and solid were separated by centrifugation, the solid was dried, and the W concentration of the solid was determined using ICP-MS.

3. Results and discussion

3.1. Oxidative cleavage of methyl 9,10-epoxystearate

In the first set of experiments, the effects of reaction time on the conversion of epoxide **1** and the yields of the aldehyde products (**2** and **3**) were investigated at temperatures ranging from 25 to 35 °C, with the results shown in Fig. 1. During the reaction process, epoxide **1** was first hydrolyzed to vic-diol **4**, followed by oxidation to give the oxygen-rich products **5**, **6**, **7** and **8**, with subsequent cleavage to generate aldehydes **2** and **3**.[32] Notably, aldehydes **2** and **3** were always generated in equimolar amounts and no over-oxidized products (that is, carboxylic acids) were obtained. As the reaction time was prolonged, the conversion of **1** and the aldehyde yields gradually increased to maximum values and then remained basically unchanged. In addition, elevating the temperature was found to increase the reaction rate. However, as the temperature was increased, the aldehydes yield decreased from 97% at 25 °C to 92% at 35 °C, likely due to enhanced thermal decomposition of the H_2O_2 at the higher temperature. Typically, >99% conversion of epoxide **1** and >90% yields of the aldehydes were observed over the temperature range of 25–35 °C for durations of 3.5–10.5 h. In past reports concerning the oxidative cleavage of methyl oleate and its derivatives to give aldehydes, Louis *et al.*[18] and Ho *et al.*[28] obtained 90% and 13% isolated yields, respectively, while Deruer *et al.*,[25] Spannring *et al.*[26] and Haimov *et al.*[29] reported GC yields (determined by gas chromatography) of 40%, 96% and 97%, respectively. For comparison purposes, WO_3 was also used as a catalyst to promote the oxidation and cleavage of epoxide **1** under the same conditions, giving an approximately 86% yield of the aldehydes following a reaction time of 10.5 h and >90% yield after 18 h. The WO_3 exhibited weaker catalytic activity than the H_2WO_4 primarily because the latter provided a more acidic environment for the oxidative cleavage reaction.[33,34]

The degree of homogeneity of the H_2WO_4 during the H_2O_2-based oxidative cleavage reaction of the EFAME was subsequently studied. As shown in Fig. 2(A1–A3), the H_2WO_4 was mixed with H_2O_2 and the color of the resulting mixture was tracked over time. The mixture was found to transition from yellow to cyan over time to eventually produce a colorless solution. In another experiment, epoxide **1** and *t*-BuOH were also included in the mixture, to reproduce the oxidative cleavage reaction solution. The color change of this mixture over time is summarized in Fig. 2(B1–B3), which shows a similar

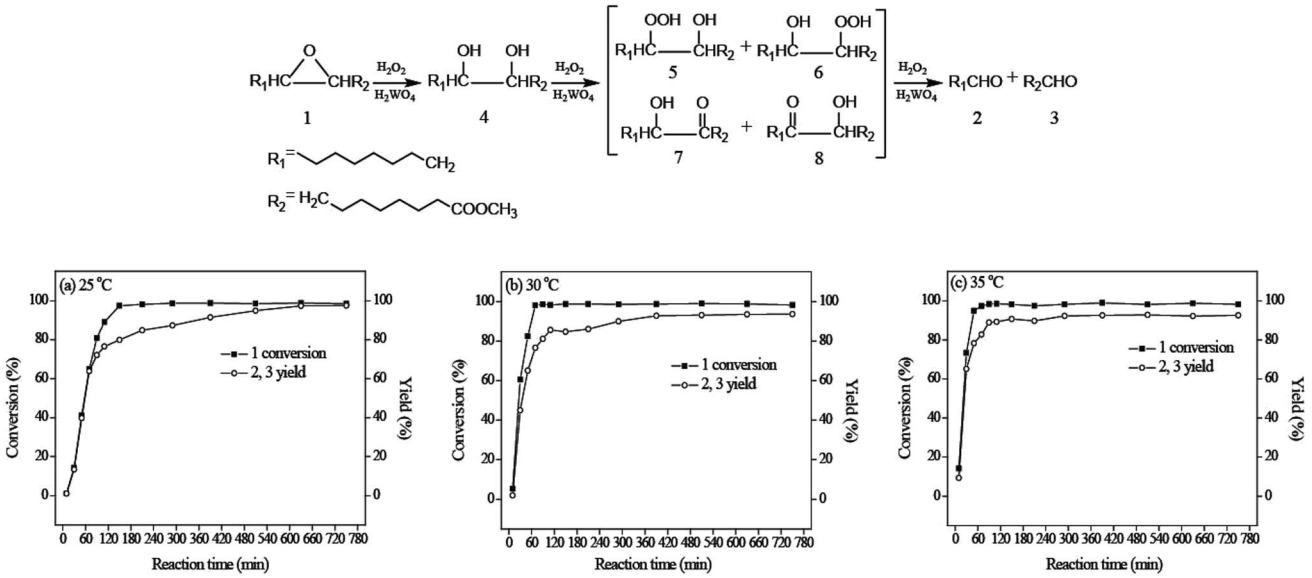

Fig. 1 Effect of reaction time on **1** conversion and aldehyde products (**2** and **3**) yields in the temperature range of 25–35 °C (10 mmol epoxide **1**, 12 mmol H_2O_2, 0.17 mmol H_2WO_4, 5 ml *t*-BuOH).

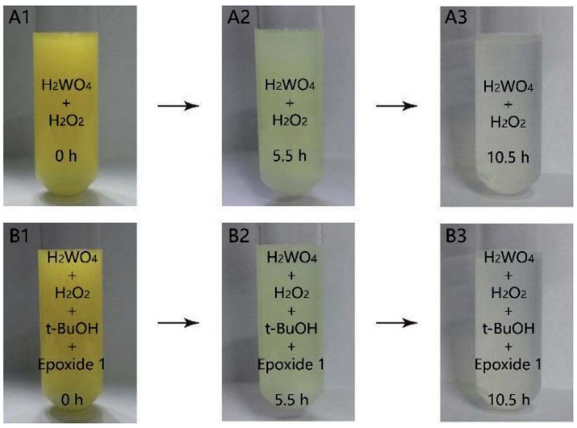

Fig. 2 Study of homogeneity or heterogeneity of H_2WO_4 in the H_2O_2-based EFAMEs oxidative cleavage reaction (25 °C, 10 mmol epoxide **1**, 12 mmol H_2O_2, 0.17 mmol H_2WO_4, 5 ml *t*-BuOH).

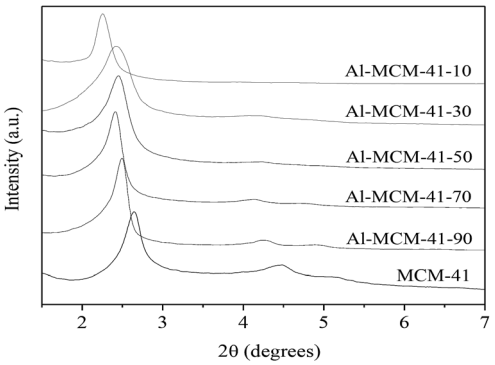

Fig. 3 The low angle XRD patterns of MCM-41 and Al-MCM-41.

trend to the experiment without the epoxide and solvent. The changes in the color of the reaction mixture indicate that the H_2WO_4 was dissolved during the reaction process, suggesting that it functioned as a homogeneous catalyst. Therefore, additional work was required to assess separation and recovery of the catalyst.

3.2. Characterization of Al-MCM-41

The actual Si/Al molar ratios of the different Al-MCM-41 samples, as determined by ICP-MS, are provided in Table 1. These ratios were relatively close to, although slightly lower than, the corresponding feed ratios. Similar differences between the actual and nominal Si/Al ratios have been previously reported. In one study, Al-MCM-41 prepared from aluminum isopropoxide and pseudo boehmite showed Si/Al molar ratios lower than the feed ratios.[44]

Fig. 3 presents the low angle XRD patterns generated by MCM-41 and Al-MCM-41 materials. All samples produced peaks characteristic of a typical mesoporous MCM-41 structure.[45] The characteristic reflections of (100), (110) and (200) crystal planes at 2θ values of 2.5°, 4.3° and 4.9° are evident, indicating the presence of a two-dimensional hexagonal lattice. With decreases in the Si/Al ratio (that is, increases in the Al content), the (110) and (200) reflections become less intense and broader, suggesting that the incorporation of Al into the silica framework disturbs the long-range order of the MCM-41.[46] Moreover, the (100) reflection shifts to smaller angles as the Si/Al ratio decreases, showing that the d_{100} spacing in the material became wider. The d_{100} spacings of the MCM-41 and Al-MCM-41 are summarized in Table 1. These data demonstrate that increases in the Al concentration increased the (100) crystal plane spacings from 3.33 nm in the pure MCM-41 to 3.86 nm in the Al-MCM-41-10. This effect is attributed to increases in the wall thickness ($t = a - d_p$, $d_{100} = a \times \sin 60°$) and the replacement of shorter Si–O bonds (0.160 nm) by longer Al–O bonds (0.175 nm) in the Al-MCM-41 structure.[47]

The nitrogen adsorption/desorption isotherms and pore size distribution curves of the MCM-41 and Al-MCM-41 are depicted in Fig. 4. All samples produced type IV isotherms, corresponding to mesoporous materials according to the IUPAC classification system.[48] In addition, the pore size distribution plots (inset to Fig. 4) demonstrate that the pore size distributions of both the MCM-41 and Al-MCM-41 were narrow and uniform. The corresponding BET specific surface areas, average pore sizes and pore volumes are summarized in Table 1. All samples had high surface areas (1011–1518 $m^2\ g^{-1}$) and suitable average pore sizes (2.68–3.34 nm). With increase in the Al concentration, the BET surface areas decreased while the average pore sizes increased, because shorter Si–O bonds were replaced by longer Al–O bonds.

Fig. 5 presents TEM images of the MCM-41 and Al-MCM-41. The MCM-41 evidently had a regular mesoporous structure with a high degree of long-range order. Following the incorporation of Al, the Al-MCM-41 was found to have a worm-like pore structure with reduced long-range order, in agreement with the

Table 1 Physiochemical properties of MCM-41 and Al-MCM-41

Samples	Si/Al molar ratio	d_{100} (nm)	BET surface area ($m^2\ g^{-1}$)	Total pore volume ($cm^3\ g^{-1}$)	Average pore diameter (nm)
Al-MCM-41-10	7	3.86	1011	0.88	3.34
Al-MCM-41-30	29	3.65	1181	0.88	2.95
Al-MCM-41-50	46	3.59	1281	1.00	2.88
Al-MCM-41-70	66	3.50	1279	0.97	2.91
Al-MCM-41-90	85	3.48	1370	0.98	2.78
MCM-41	—	3.33	1518	1.04	2.68

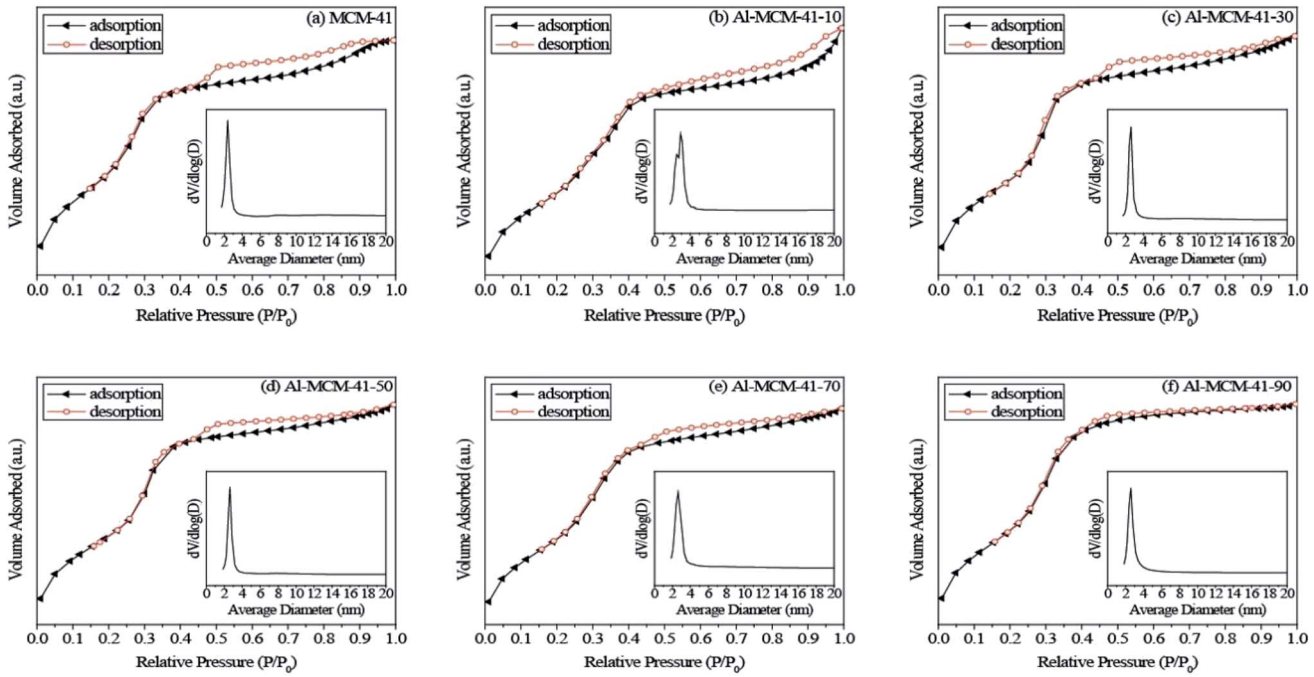

Fig. 4 The nitrogen adsorption/desorption isotherms and pore size distribution curves of MCM-41 and Al-MCM-41.

weaker (110) and (200) crystal planes reflections in the low angle XRD patterns of these materials (Fig. 3).

The acidities of MCM-41 and Al-MCM-41 solids were measured by thermoprogrammed desorption of Py followed by FTIR spectroscopy, and quantitative data regarding Brønsted and Lewis acid sites on the samples are provided in Table 2. With increases in the Si/Al ratio, the acidity of the samples decreased as a result of the lower Al concentrations. Assessing pyridine desorption at different temperatures thus provided useful information that allowed a qualitative evaluation of the strengths of acid sites.[49] All Al-MCM-41 samples lost approximately 80% of their Brønsted acid sites after desorption at 350 °C, showing that these materials possessed weak to moderate Brønsted acidity. In contrast, approximately half of the Lewis acid sites were retained in the Al-MCM-41 samples after desorption at 350 °C, demonstrating the presence of strong Lewis acid sites in these substances. The MCM-41 was found to have only weak Lewis acidity.

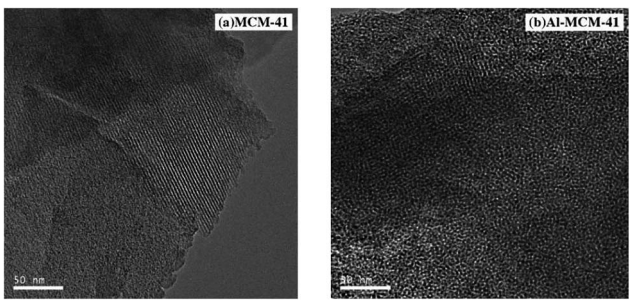

Fig. 5 TEM images of (a) MCM-41 and (b) Al-MCM-41.

3.3. PZC values of Al-MCM-41 and W-containing anion adsorption

Al_2O_3 typically has a high PZC value within a wide range from 5.0 to 9.6, while the PZC values of SiO_2 materials are usually below 4.0.[36] Fig. 6(a) shows the effect of the Al content on the PZC value of Al-MCM-41. With decreases in the Si/Al ratio, the PZC value was increased. This PZC value was also closely related to the anion adsorption performance of the material. Theoretically, a higher PZC value will be associated with better adsorption performance. Fig. 6(b) compares the W-containing anion absorptions of the MCM-41 and Al-MCM-41, based on determining the W levels in these materials after adsorption, using ICP-MS. As expected, the Al-MCM-41 exhibited better adsorption performance than the MCM-41 and the quantity of anions adsorbed by the Al-MCM-41 increased as the Si/Al ratio decreased (that is, with increasing PZC values).

Table 2 Acidity of MCM-41 and Al-MCM-41 measured by FTIR of adsorbed pyridine at different temperatures

	Concentration of acid sites, $\mu mol_{pyridine}/g_{support}$					
	Brønsted sites			Lewis sites		
Samples	150 °C	250 °C	350 °C	150 °C	250 °C	350 °C
Al-MCM-41-10	59	40	9	76	55	50
Al-MCM-41-30	40	25	10	42	30	25
Al-MCM-41-50	36	23	5	24	19	18
Al-MCM-41-70	31	23	4	22	15	11
Al-MCM-41-90	21	15	4	8	6	3
MCM-41	0	0	0	28	0	0

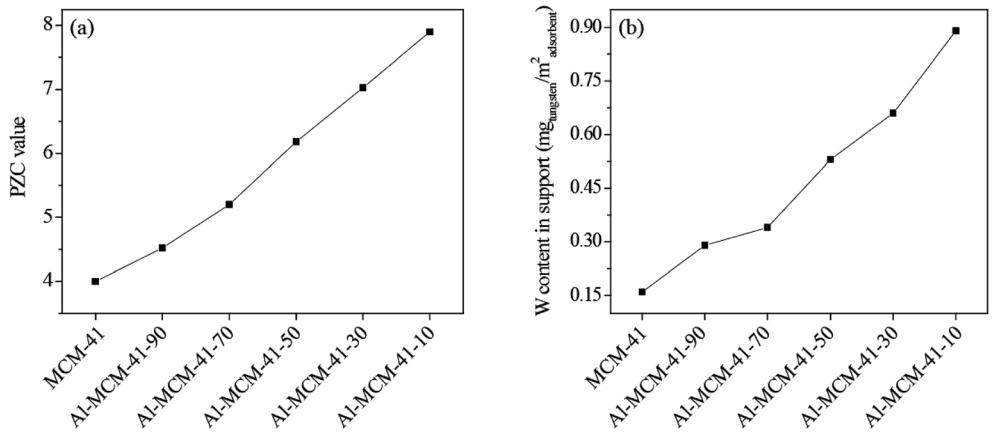

Fig. 6 (a) PZC values of MCM-41 and Al-MCM-41; (b) absorption performance of MCM-41 and Al-MCM-41 to tungsten-containing anion.

3.4. Effects of MCM-41 and Al-MCM-41 on the oxidative cleavage of methyl 9,10-epoxystearate

In the experiments, MCM-41 and Al-MCM-41 as adsorbent were directly added into the reaction mixture and were always present until the end of the reaction, so the effect of MCM-41 and Al-MCM-41 on oxidative cleavage of epoxide **1** could not be ignored. The potential for decomposition of the H_2O_2 by these materials was assessed by mixing either the MCM-41 or Al-MCM-41 with H_2O_2 and allowing the resulting mixture to stir at ambient temperature, after which a potassium permanganate titration was used to determine the concentration of H_2O_2. As shown in Fig. 7(a), after 12 h, the H_2O_2 concentration was essentially unchanged, indicating that neither the MCM-41 nor the Al-MCM-41 promoted decomposition of the H_2O_2. In an industrial operation, H_2O_2 is often stored at room temperature in aluminum tanks, because aluminum forms a hydrated alumina film in contact with the H_2O_2 solution. This film hinders the decomposition of H_2O_2 by separating the H_2O_2 from the bare metal. Moreover, The effect of the acidity of both the MCM-41 and Al-MCM-41 on the oxidative cleavage of epoxide **1** was studied, and the results are presented in Fig. 7(b). The addition of either MCM-41 or Al-MCM-41 to the reaction mixture had no significant effect on either the epoxide **1** conversion or the aldehydes yield (see Fig. 1). This lack of an effect can possibly be attributed to the ability of the H_2WO_4 to provide sufficient acidity for the reaction to proceed.

3.5. Recycling of the catalyst

Fig. 8 summarizes the reusability of the H_2WO_4 catalyst after adding MCM-41 or Al-MCM-41 following the oxidative cleavage of epoxide **1** into bio-based aldehydes. During the first recycling experiment, the H_2WO_4 and MCM-41, or Al-MCM-41, were added together before the start of the reaction. During the reaction, the H_2WO_4 was initially transformed into the peroxo-W anion $[W_xO_y(O_2)_z]^{n-}$ which acted as the active component and then reduced to the soluble anion $[W_xO_y]^{n-}$ after reaction.[23,35,50] The hydroxyl groups on the MCM-41 and Al-MCM-41 surfaces would have interacted with hydrogen ions and so carried positive charges, allowing these materials to absorb the W-containing anions. The MCM-41 and Al-MCM-41 holding the adsorbed anions (designated H_2WO_4@MCM-41 and H_2WO_4@Al-MCM-41) were separated from the reaction

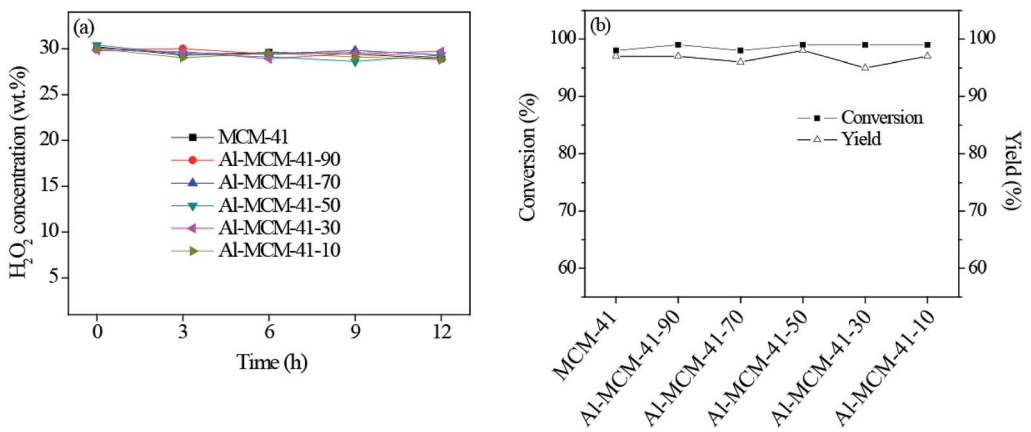

Fig. 7 (a) Effect of MCM-41 and Al-MCM-41 on H_2O_2; (b) effect of the acidity of MCM-41 and Al-MCM-41 on epoxide **1** conversion and aldehyde products (**2** and **3**) yields (25 °C, 10.5 h, 10 mmol epoxide **1**, 12 mmol H_2O_2, 0.17 mmol H_2WO_4, 5 ml *t*-BuOH, 100 mg MCM-41 or Al-MCM-41).

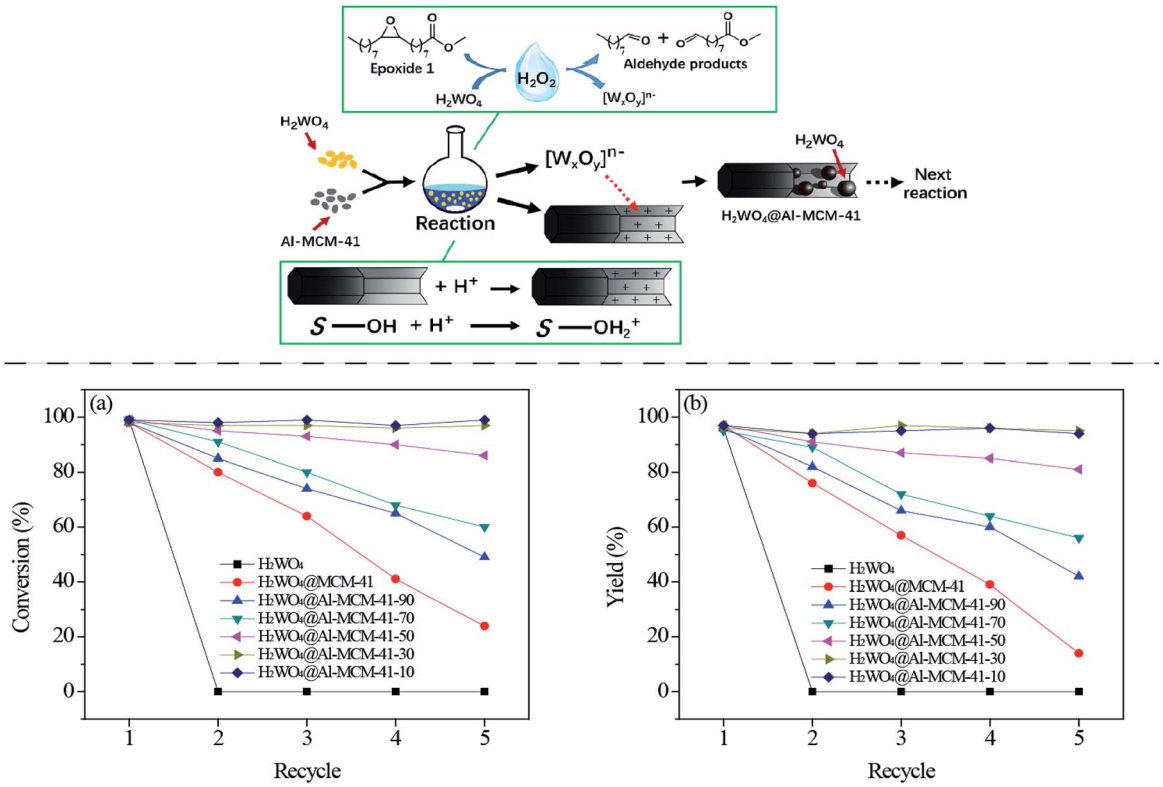

Fig. 8 Recycle of catalyst after adding MCM-41 and Al-MCM-41 (25 °C, 10.5 h, 10 mmol epoxide **1**, 12 mmol H_2O_2, 0.17 mmol H_2WO_4, 5 ml *t*-BuOH, 100 mg MCM-41 or Al-MCM-41).

solution, washed with *t*-BuOH, dried at ambient temperature and reused in a subsequent reaction. The pure H_2WO_4 was dissolved in the reaction solution and thus could only be used once. The H_2WO_4@MCM-41 and H_2WO_4@Al-MCM-41 both showed good reusability, primarily due to the adsorption and immobilization of dissolved W species on these materials. Moreover, the catalyst reusability was increased as the Al concentration in the Al-MCM-41 increased. When using Al-MCM-41-10 or Al-MCM-41-30 as adsorbents, no W species were detected in the liquid product during ICP-MS analyses, and there was no significant decrease in catalytic activity after five recycling experiments.

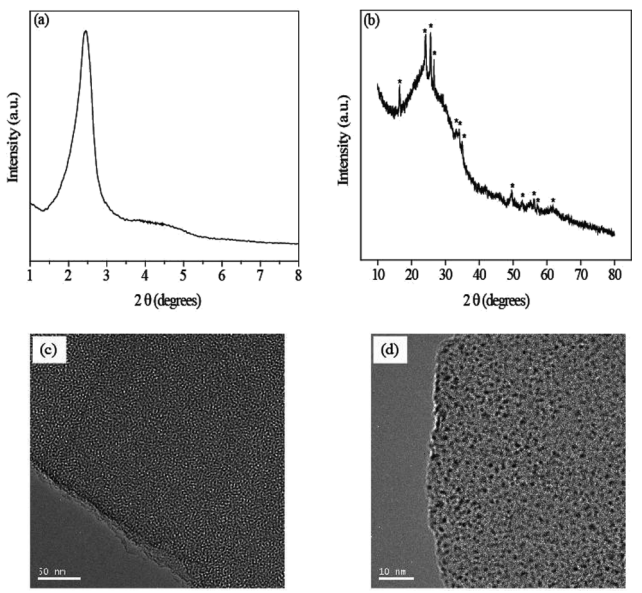

Fig. 9 The XRD patterns ((a) and (b)) and TEM images ((c) and (d)) of the recovered H_2WO_4@Al-MCM-41-10.

The H_2WO_4@Al-MCM-41 was characterized using both XRD and transmission electron microscopy (TEM). The resulting low angle XRD pattern is presented in Fig. 9(a), which suggests that the recovered H_2WO_4@Al-MCM-41 still has a good mesoporous structure. The wide angle XRD pattern in Fig. 9(b) exhibits peaks at 2θ values of 16.49°, 24.16°, 25.62°, 26.63°, 33.24°, 34.04°, 35.02°, 49.63°, 52.71°, 56.18°, 57.20° and 61.23°, corresponding to orthorhombic H_2WO_4 (ICDD-PDF no. 84-0886). The TEM image of the recovered H_2WO_4@Al-MCM-41 in Fig. 9(b) confirms that the pore structure of the Al-MCM-41 was not significantly modified after adsorption of the H_2WO_4, and that H_2WO_4 particles approximately 1 nm in size were uniformly adsorbed and well dispersed on the Al-MCM-41.

4. Conclusions

H_2WO_4 was used as a catalyst to promote the oxidation and cleavage of methyl 9,10-epoxystearate into the corresponding free aldehydes, employing H_2O_2 as the oxidant with *t*-BuOH as the solvent. Using a 10/12/0.17 (on a mmol basis) mixture of

epoxide/H_2O_2/H_2WO_4 and 5 ml of *t*-BuOH, >99% conversion and >90% yield were obtained over the temperature range of 25–35 °C with durations of 3.5–10.5 h. The H_2WO_4 was found to dissolve in the reaction mixture and thus showed the characteristics of a homogeneous catalyst. A series of Al-MCM-41 materials having different Si/Al molar ratios (from 10 to 90) were prepared and introduced into the reaction system to allow recovery of the catalyst by adsorption of dissolved W species. Characterization by ICP-MS, XRD, BET, TEM and Py-FTIR was performed to study the physiochemical properties of the Al-MCM-41, and PZC values were also determined by salt titration. The results show that each of the Al-MCM-41 materials exhibited typical MCM-41 characteristics. The incorporation of Al disturbed the long-range order of the MCM-41 but increased the PZC value. The Al-MCM-41-10 and Al-MCM-41-30 possessed the highest PZC values and showed the optimal W anion adsorption performance. After adding the Al-MCM-41-10 or Al-MCM-41-30, the catalyst could be reused five times without any significant loss of activity.

Conflicts of interest

There are no conflicts to declare.

Acknowledgements

This work was supported by the Zhejiang Science and Technology Plan Project (Fund number: 2017C37054). Thanks for financial support by Zhejiang Ministry of Science and Technology. We also thank Liwen Bianji, Edanz Editing China (www.liwenbianji.cn/ac), for editing the English text of a draft of this manuscript.

References

1 Y. Zhu, C. Romain and C. K. Williams, *Nature*, 2016, **540**, 354–362.
2 A. E. Kerenkan, F. Béland and T. Do, *Catal. Sci. Technol.*, 2016, **6**, 971–987.
3 AOCS lipid library, http://lipidlibrary.aocs.org/market/nonfood.htm.
4 Z. Wu, J. Fang, Q. Xie, T. Zheng, L. Wu, M. Lu, L. Zhang, Y. Nie and J. Ji, *Ind. Crops Prod.*, 2018, **122**, 266–276.
5 A. Köckritz and A. Martin, *Eur. J. Lipid Sci. Technol.*, 2008, **110**, 812–824.
6 J. M. Fraile, J. I. García, C. I. Herrerías and E. Pires, *Synthesis*, 2017, **49**, 1444–1460.
7 Z. Wu, T. Zheng, L. Wu, H. Lou, Q. Xie, M. Lu, L. Zhang, Y. Nie and J. Ji, *Ind. Eng. Chem. Res.*, 2017, **56**, 5231–5238.
8 M. Guidotti, R. Psaro, N. Ravasio, M. Sgobba, E. Gianotti and S. Grinberg, *Catal. Lett.*, 2007, **122**, 53–56.
9 S. Sankaranarayanan, A. Sharma and K. Srinivasan, *Catal. Sci. Technol.*, 2015, **5**, 1187–1197.
10 P. K. Khatri, M. Aila, J. Porwal, S. Kaul and S. L. Jain, *New J. Chem.*, 2015, **39**, 5960–5965.
11 P. Neves, T. R. Amarante, A. A. Valente, M. Pillinger and I. S. Gonçalves, *Catal. Lett.*, 2016, **146**, 841–850.
12 G. Du, A. Tekin, E. G. Hammond and L. K. Woo, *J. Am. Oil Chem. Soc.*, 2016, **81**, 477–480.
13 E. Poli, J. M. Clacens, J. Barrault and Y. Pouilloux, *Catal. Today*, 2009, **140**, 19–22.
14 E. Milchert, K. Malarczyk and M. Kłos, *Molecules*, 2015, **20**, 21481–21493.
15 A. Rubinstein, R. Carmeli and R. Neumann, *Chem. Commun.*, 2014, **50**, 13247–13249.
16 M. Sutter, W. Dayoub, E. Métay, Y. Raoul and M. Lemaire, *Green Chem.*, 2013, **15**, 786–797.
17 Y. Shi, W. Dayoub, G. Chen and M. Lemaire, *Green Chem.*, 2010, **12**, 2189–2195.
18 K. Louis, L. Vivier, J. Clacens, M. Brandhorst, J. Dubois, K. D. O. Vigier and Y. Pouilloux, *Green Chem.*, 2014, **16**, 96–101.
19 P. H. Hoang, N. T. Nhung and L. Q. Dien, *AIP Adv.*, 2017, **7**, 105311.
20 A. S. Ello, A. Enferadi-kerenkan, A. Trokourey and T. Do, *J. Am. Oil Chem. Soc.*, 2017, **94**, 1451–1461.
21 A. Behr, N. Tenhumberg and A. Wintzer, *RSC Adv.*, 2013, **3**, 172–180.
22 B. R. Travis, R. S. Narayan and B. Borhan, *J. Am. Chem. Soc.*, 2002, **124**, 3824–3825.
23 M. Lu, L. Peng, Q. Xie, N. Yang, H. Jin, Z. Wu, Y. Nie, X. Liu, X. Lu and J. Ji, *Green Chem.*, 2019, **21**, 560–566.
24 P. Spannring, P. C. A. Bruijnincx, B. M. Weckhuysen and R. J. M. K. Gebbink, *Catal. Sci. Technol.*, 2014, **4**, 2182–2209.
25 E. Deruer, N. Duguet and M. Lemaire, *ChemSusChem*, 2015, **8**, 2481–2486.
26 P. Spannring, V. Yazerski, P. C. A. Bruijnincx, B. M. Weckhuysen and R. J. M. KleinGebbink, *Chem.–Eur. J.*, 2013, **19**, 15012–15018.
27 C. M. P. Cecchi, D. Cesarín-Sobrinho, A. B. B. Ferreira and J. C. Netto-Ferreira, *Catalysts*, 2018, **8**, 6.
28 C. Ho, W. Yu and C. Che, *Angew. Chem., Int. Ed.*, 2004, **43**, 3303–3307.
29 A. Haimov, H. Cohen and R. Neumann, *J. Am. Chem. Soc.*, 2004, **126**, 11762–11763.
30 M. Lu, L. Peng, Q. Xie, Y. Nie, X. Liu, X. Lu and J. Ji, *Eur. J. Lipid Sci. Technol.*, 2018, **120**, 1700415.
31 M. Wang, J. Ma, H. Liu, N. Luo, Z. Zhao and F. Wang, *ACS Catal.*, 2018, **8**, 2129–2165.
32 E. Antonelli, R. D'Aloisio, M. Gambaro, T. Fiorani and C. Venturello, *J. Org. Chem.*, 1998, **63**, 7190–7206.
33 P. Spannring, I. Prat, M. Costas, M. Lutz, P. C. A. Bruijnincx, B. M. Weckhuysen and R. J. M. K. Gebbink, *Catal. Sci. Technol.*, 2014, **4**, 708–716.
34 I. R. Piletic, E. O. Edney and L. J. Bartolotti, *Phys. Chem. Chem. Phys.*, 2013, **15**, 18065–18076.
35 Y. Yoshimura, Y. Ogasawara, K. Suzuki, K. Yamaguchi and N. Mizuno, *Catal. Sci. Technol.*, 2017, **7**, 1662–1670.
36 M. Kosmulski, *J. Colloid Interface Sci.*, 2004, **275**, 214–224.
37 C. Sun and J. C. Berg, *Adv. Colloid Interface Sci.*, 2003, **105**, 151–175.
38 A. Hiroki and J. A. LaVerne, *J. Phys. Chem. B*, 2005, **109**, 3364–3370.

39 H. Ziaei-Azad, J. M. Kolle, N. Al-Yasser and A. Sayari, *Microporous Mesoporous Mater.*, 2018, **262**, 166–174.
40 M. Lu, X. Liu, Y. Li, Y. Nie, X. Lu, D. Deng, Q. Xie and J. Ji, *J. Renew. Sustain. Energy*, 2016, **8**, 053103.
41 Z. Wu, Y. Nie, W. Chen, L. Wu, P. Chen, M. Lu, F. Yu and J. Ji, *Can. J. Chem. Eng.*, 2016, **94**, 1576–1582.
42 C. A. Emeis, *J. Catal.*, 1993, **141**, 347–354.
43 K. Sakurai, Y. Ohdate and K. Kyuma, *Soil Sci. Plant Nutr.*, 1988, **34**, 171–182.
44 K. M. Reddy and C. Song, *Catal. Lett.*, 1996, **36**, 103–109.
45 J. S. Beck, J. C. Vartuli, W. J. Roth, M. E. Leonowicz, C. T. Kresge, K. D. Schmitt, C. T.-W. Chu, D. H. Olson, E. W. Sheppard, S. B. McCullen, J. B. Higgins and J. L. Schlenker, *J. Am. Chem. Soc.*, 1992, **114**, 10834–10843.
46 X. Chen, L. Huang, G. Ding and Q. Li, *Catal. Lett.*, 1997, **44**, 123–128.
47 R. B. Borade and A. Clearfield, *Catal. Lett.*, 1995, **31**, 267–272.
48 K. S. W. Sing, D. H. Everett, R. A. W. Haul, L. Moscou, R. A. Pierotti, J. Rouquérol and T. Siemieniewska, *Pure Appl. Chem.*, 1985, **57**, 603–619.
49 H. Ziaei-Azad and A. Sayari, *J. Catal.*, 2016, **344**, 729–740.
50 E. Lassner, and W. Schubert, *Tungsten: Properties, Chemistry, Technology of the Element, Alloys, and Chemical Compounds*, Kluwer Academic/Plenum Publishers, New York, 1999, pp. 53–122.